Electronic Supplementary Material (ESI) for Nanoscale.


# Supporting Information:

# Defect Engineering for Thermal Transport Properties of Nanocrystalline Molybdenum Diselenide

## 1 Contents

Here is the outline of the supporting information. First, atomic coordinates of are shown in for polycrystalline monolayer and monocrystalline sample with point vacancies. The following section shows a flow chart of the annealing process. In the next section, atomic velocity distribution is compared with Maxwell–Boltzmann distribution as a metric to validate achievement of sufficient sample relaxation. Next, temperature profile and heat flux of pristine and polycrystalline samples are illustrated. Then, thermal conductivity of pristine sample is graphed as a function of sample length. Finally, further evidence of microstructural evolution is shown along with simulated X-ray spectrum and diffraction pattern during the annealing process.

## 2 $MoSe_2$ Sample With Defects

For clear visualization of grains in $40\times40$ nm$^2$ sample Figure S.1 represents samples studied in this research. Ovito program was used to visualize the sample. Polycrystalline samples have been generated by selection of uniformly distributed random coordinates for center of each grain and the vertices of grain boundaries via Voronoi tessellation algorithm. In the next step, pre-generated pristine atomic coordinates were rotated (angular misorientation is a gaussian random variable) and then these coordinates were inserted inside each grain while the atoms outside of the corresponding crystal were deleted (So tilted grain boundaries were formed). After completing this process for all the existing grains, all the atoms along the grain boundaries were inspected systematically to search for the atoms with overlapping

distances of less than 0.08 nm (Those atoms were removed from the system). Energy minimization and relaxation are not applied to any sample at this stage yet. Samples with point vacancies are generated via uniform randomization algorithms points, the minimum distance between two neighboring vacancies exceeds 0.9 nm to prevent the formation of cluster defects. In addition, the hot and cold sources (See Figure S.1) were deliberately kept free of vacancies to maintain their structural integrity and to prevent any potential disruptions in thermal behavior. Additionally, to maintain the integrity of the microstructure, it is ensured that there were no initial vacancies at the two outer edges of the ribbon, near the periodic boundaries and perpendicular to the direction of heat flux. This precautionary measure was implemented to avoid possible instability or undesirable effects that may arise due to the proximity of vacancies near periodic boundary conditions. The stability of the microstructure is then verified through multiple simulations with different initial random seed numbers for initial atomic velocities.

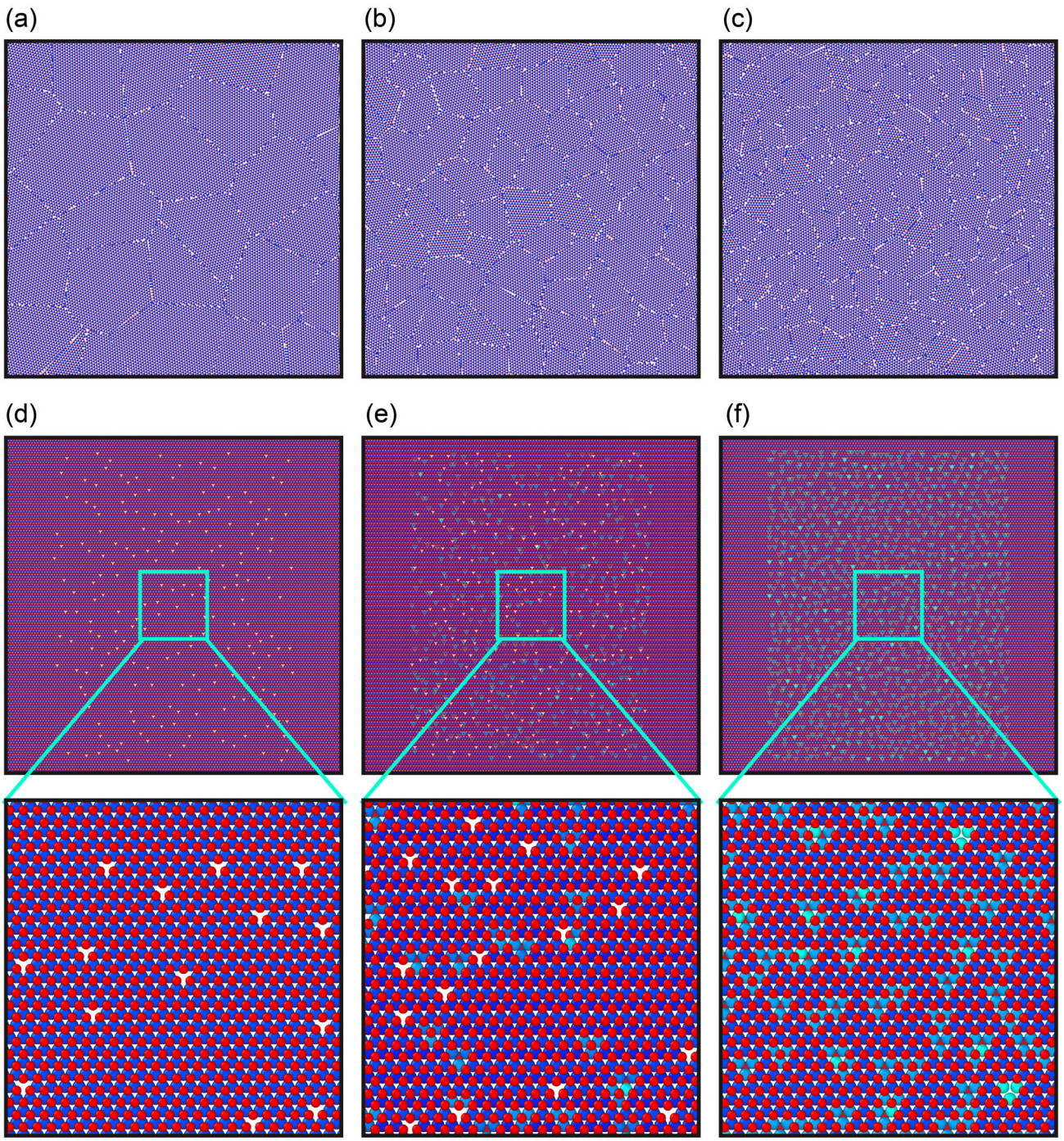


**Figure S.1:** (a-c) Schematic of $40 \times 40 nm^2$ polycrystalline $MoSe_2$ with the average grain size of 11 nm, 7 nm and 3 nm and average grain misorientation of $30^\circ$, (d-f) Samples with point vacancies where (d) is a sample with Se vacancies, (e) is a sample with Mo vacancies and (f) is sample with Mo-Se vacancies, blue atoms, yellow atoms and purple atoms represent Se in the top layer, Se in the lower layer and Mo, respectively.

# 3 Annealing Process

The annealing process is essential in sample preparation before heat transfer simulation in NEMD. To gain a better insight in the annealing process, Figure S.2 illustrates a flow chart at every 0.5 ns step.

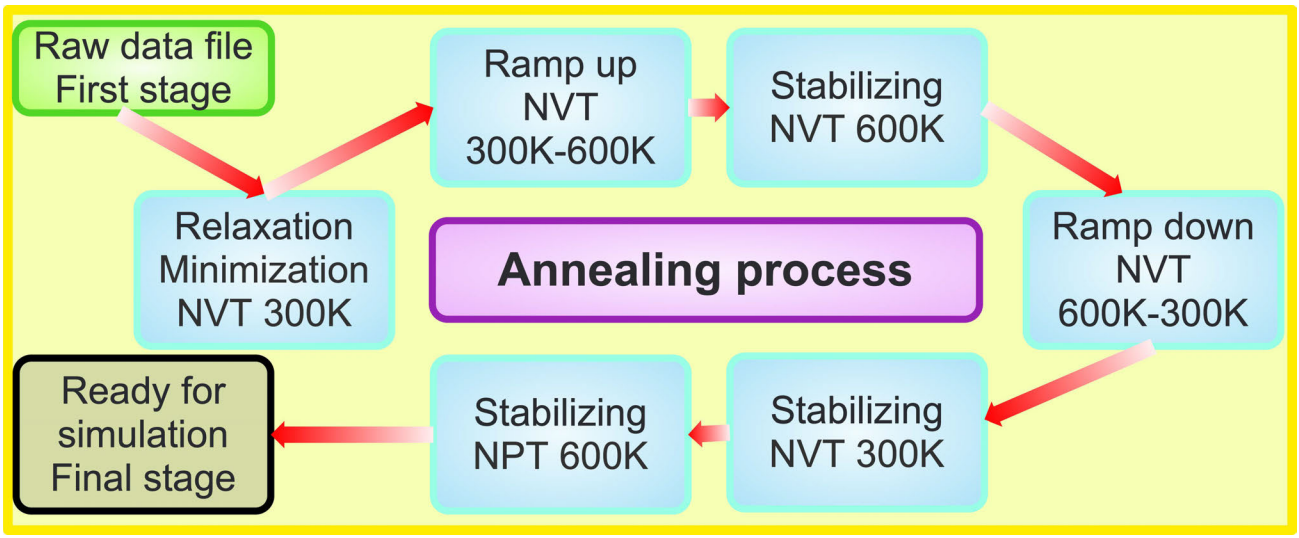


**Figure S.2:** Flow chart of the annealing prosses in polycrystalline $MoSe_2$.

# 4 Energy Relaxation

This section shows the plots of atomic velocity distribution as one indication to validate sufficient sample energy relaxation. Maxwellian probability density function is in the form of:

$$f(v) = \left(\frac{m}{2\pi kT}\right)^{3/2} 4\pi v^2 e^{-\frac{mv^2}{2kT}}, \qquad \text{(Eq S.1)}$$

Where m is atomic mass and k is Boltzmann constant. After conducting primary steps to achieve structural relaxation. As shown in FigureS.3, there is less than 1% deviation from Maxwellian distribution of atomic velocities.

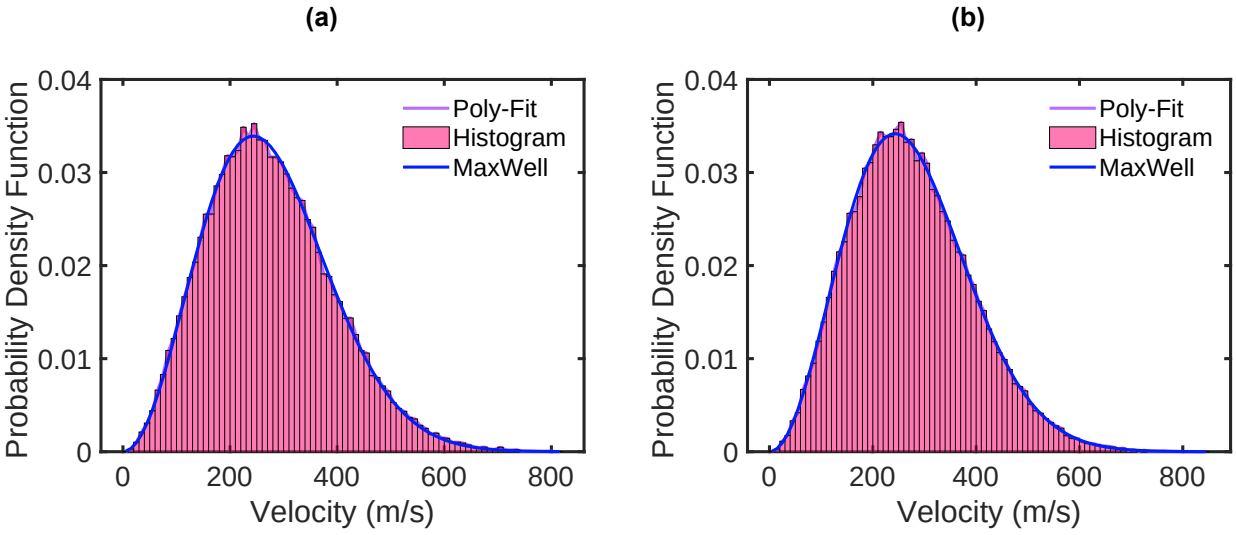


**Figure S.3:** (a) Maxwell–Boltzmann distribution of atomic velocity in single crystalline $MoSe_2$ after relaxation, (b) Maxwell– Boltzmann distribution of atomic velocity in polycrystalline after relaxation.

# 5 Temperature and Heat Flux Profiles

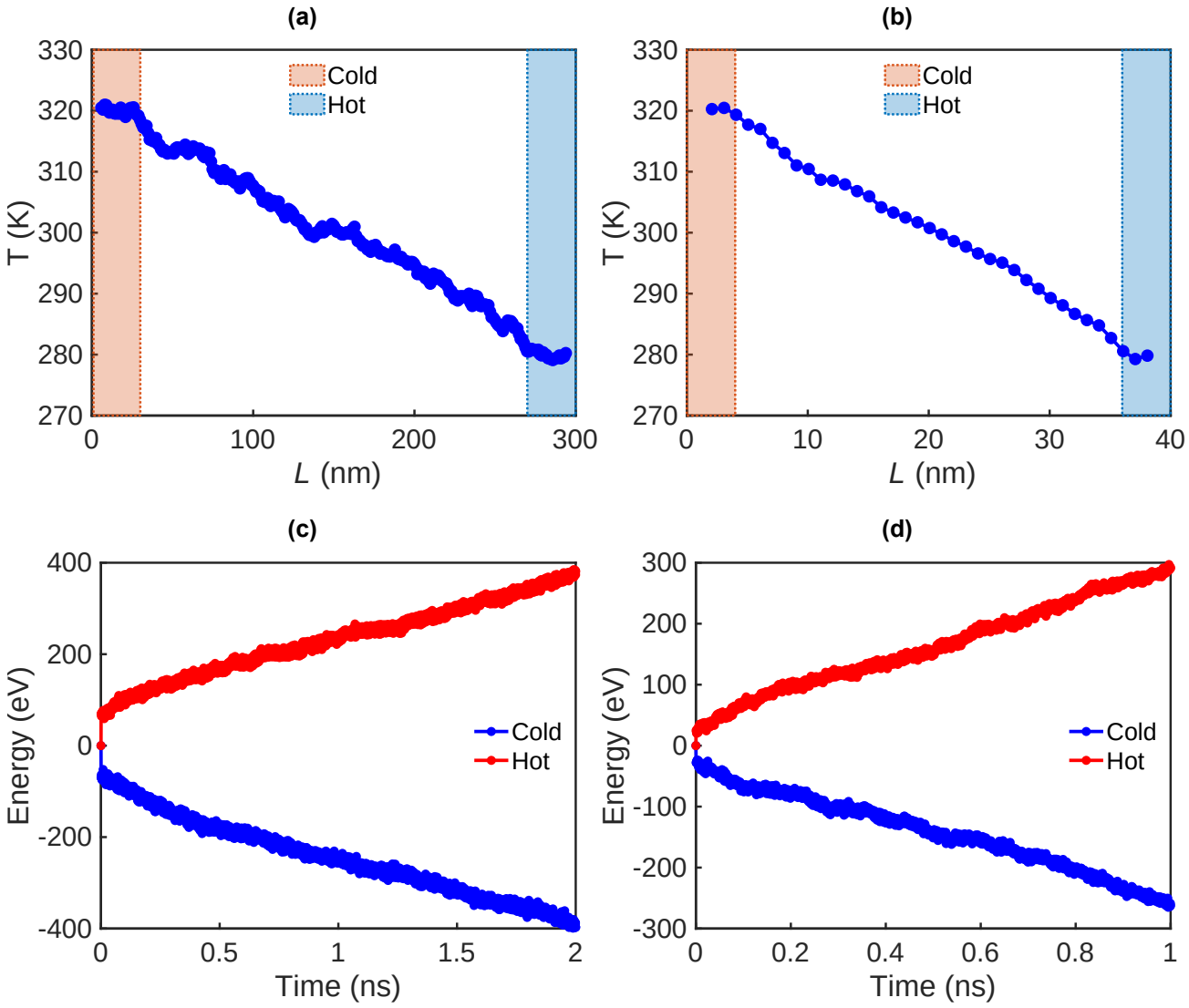


**Figure S.4:** (a-b) Temperature profile of single crystal ($L$= 300 nm) and cumulative energy of hot and cold source in single crystal sample, (c-d) Temperature profile of polycrystalline $MoSe_2$ with $\bar{d}$= 3 nm and cumulative energy of hot and cold source.

# 6 Thermal properties in Pristine$MoSe_2$ (No defects)

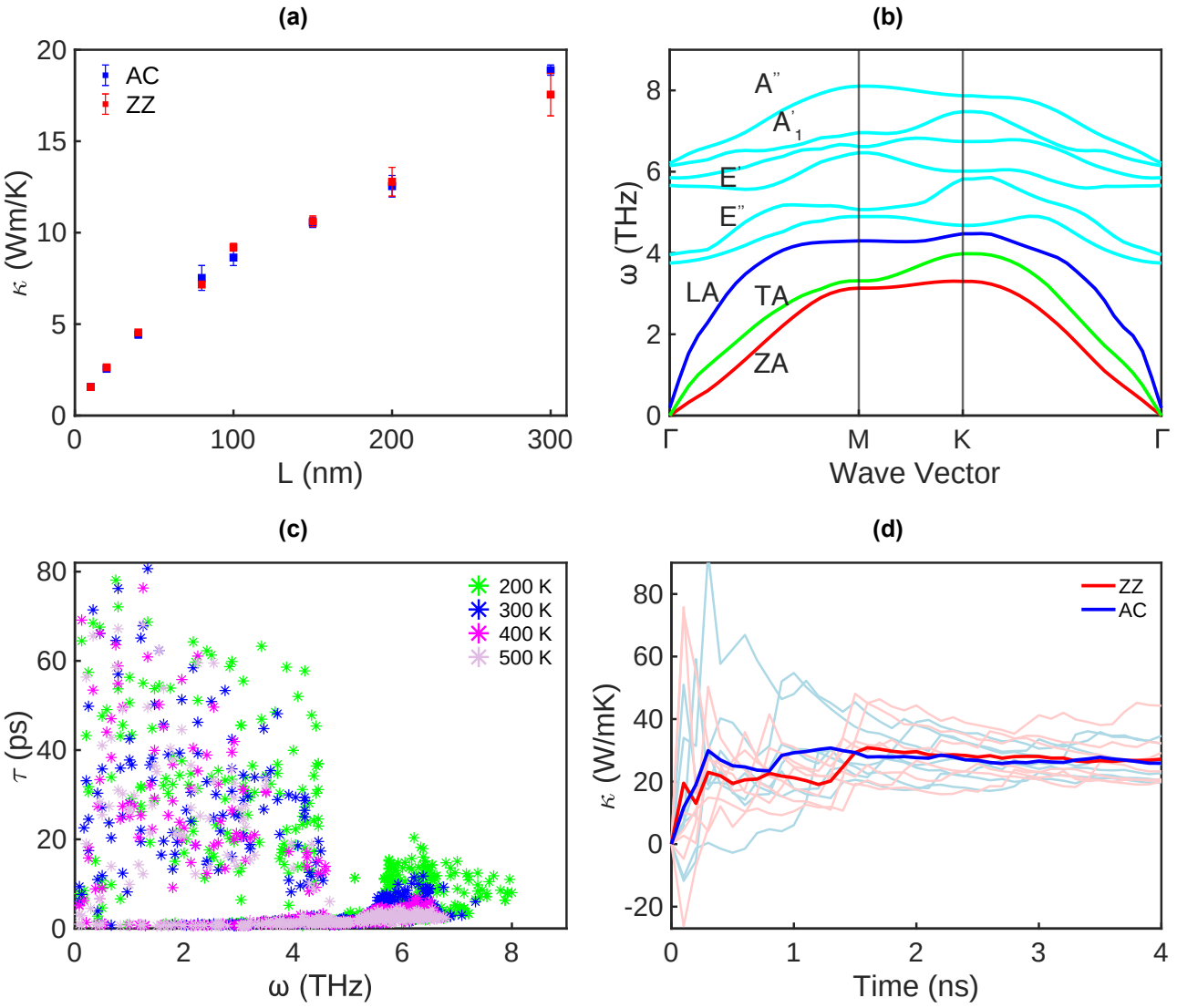


**Figure S.5:** (a) Thermal conductivity of pristine single-layer $MoSe_2$ as a function of sample length. (b) Phonon dispersion curves of pristine single layer $MoSe_2$. (c) Phonon lifetime of pristine single layer $MoSe_2$ as a function of temperature. (d) Thermal conductivity dependency on time for monolayer $MoSe_2$ in AC and ZZ directions in the EMD simulation using Green–Kubo method.

Unlike phonon dispersion curve obtained from spectral energy density (See figure 3 (d) in the manuscript), phonon dispersion calculated via Phonon package exhibits some outlier data points, thereby making the interpolation process less reliable. As such, this induced

artifact hinders the AZ branch of phonon dispersion curve from being a quadratic function near the Gamma region.

# 7 Microstructural Evolution in polycrystalline $MoSe_2$

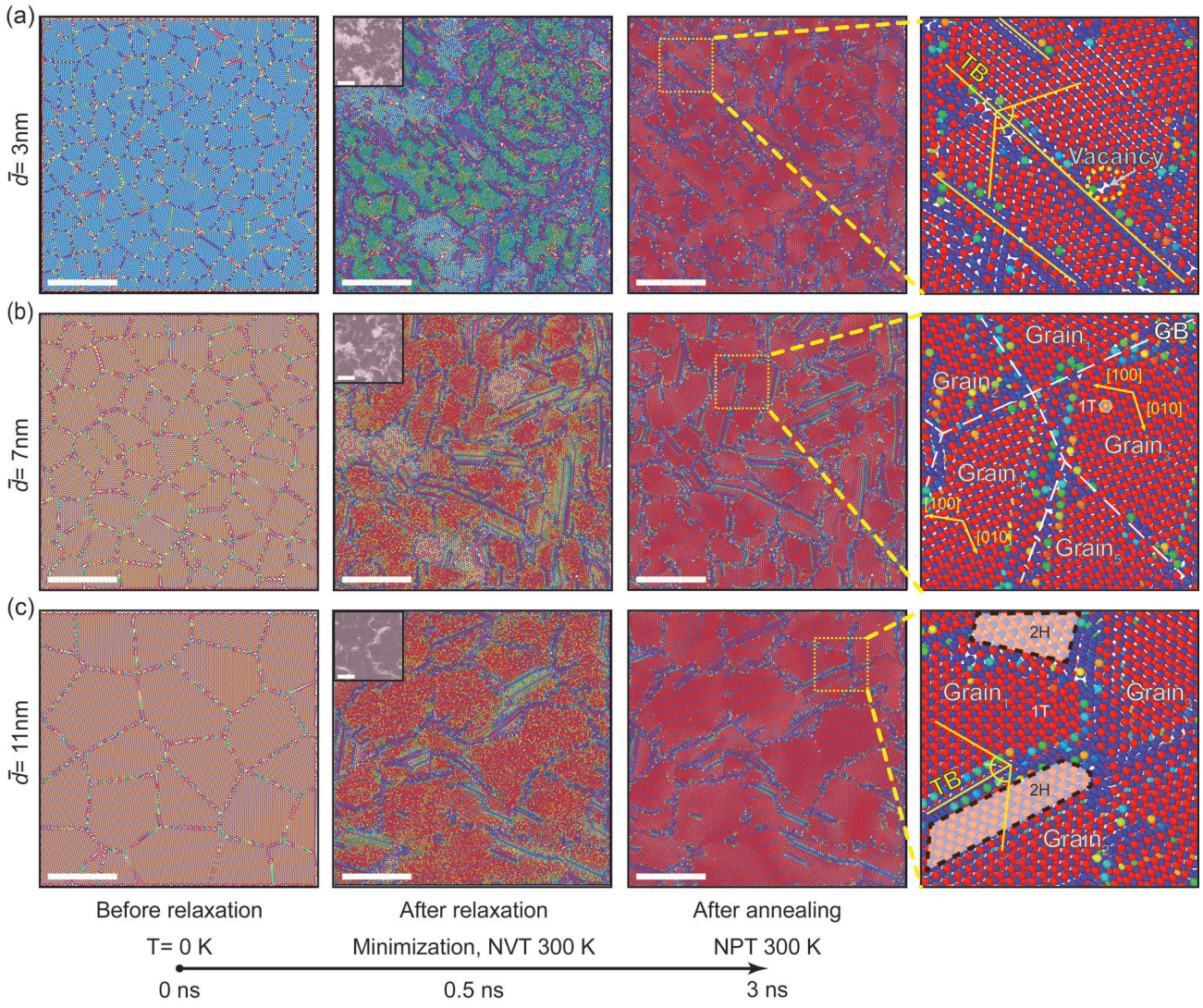


**Figure S.6:** (a) Significant phase transformation of polycrystalline $MoSe_2$ with $\bar{d}$ = 3 nm. Note that twin boundary and phase 1T formed only after the first stage of simulation. Localized high stress triggers the formation of some recoverable twin boundaries some of which disappears after stress removal as shown in the magnified region, (b) Phase transformation in polycrystalline $MoSe_2$ with $\bar{d}$ = 7 nm, magnified area shows grain boundaries and crystals (c) Phase transformation of polycrystalline $MoSe_2$ with $\bar{d}$ = 11 nm, dark blue and purple regions correspond to the locations of twin boundaries and grain boundaries. magnified area labels twin boundaries (mirroring effect) and 1T phase, color coding is based on atomic volume, inset is phase map light pink is the 2H phase, and dark pink is the 1T phase, the average angle of grain misorientation is 30° in all samples, all scale bars are 10 nm, oversizedwhite areas are vacancy defects.

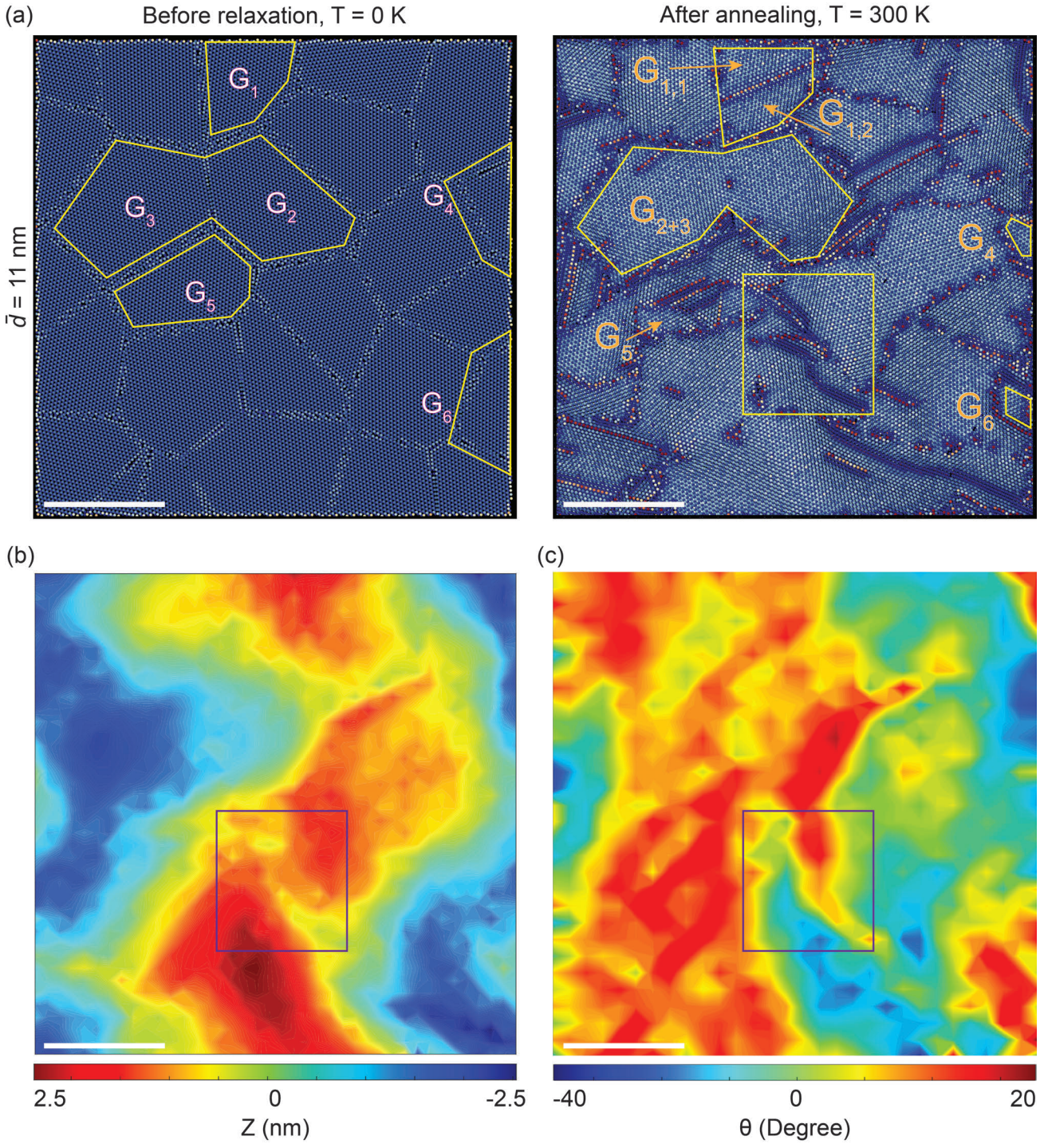


**Figure S.7:** (a) Images of polycrystalline $MoSe_2$ ($\bar{d}$ = 11 nm) before and after annealing, showing variations in grain morphology. $G_1$ splits into two smaller subgrains $G_{1,1}$ and $G_{1,2}$. $G_2$ and $G_3$ coalesced to form a larger grain $G_{2+3}$. $G_4$, $G_5$ and $G_6$ shrinks under compression. (b) Schematic representation of the out-of-plane coordinates of the sample after annealing, highlighting the variations in height and wrinkles across the sample. (c) Surface gradient map of the sample after annealing with respect to the XY plane. Scale bar is 10 nm.

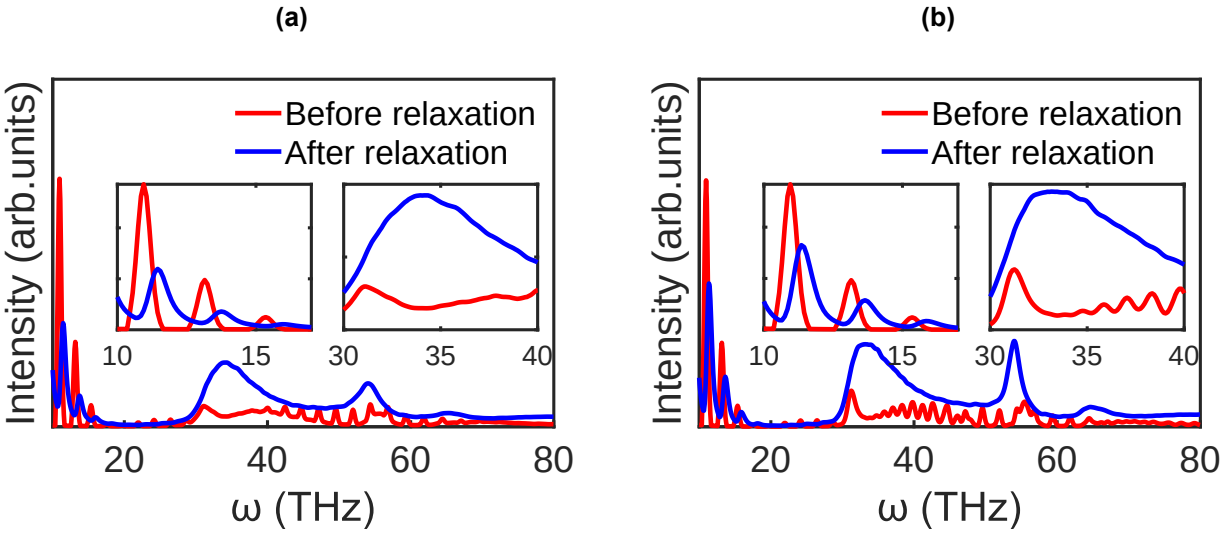


**Figure S.8:** (a) X-ray diffraction (XRD) of polycrystalline $MoSe_2$ with $\bar{d}$ = 3 nm, showing a slight the grain rotation during the annealing process (less than 1°). (b) XRD of polycrystalline $MoSe_2$ with $\bar{d}$ = 11 nm, with $\bar{\sum}$ of 30° for all the samples.

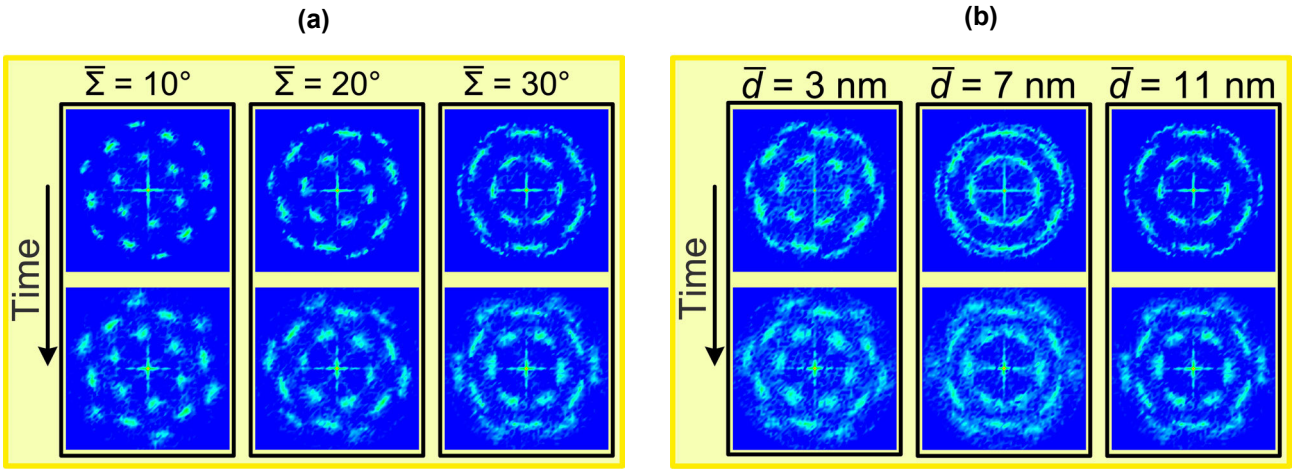


**Figure S.9:** (a) Diffraction pattern in polycrystalline $MoSe_2$ with $\bar{d}$ = 11 nm grain size before and after the annealing process varies from 10°, to 30°, (b) Diffraction pattern for a sample with $\bar{d}$ = 3 nm, $\bar{d}$ = 7 nm and $\bar{d}$ = 11 nm where average misorientation is held constant ($\bar{\sum}$ = 30°) before and after the annealing process. Diffraction patterns show that the lattice constant reduces slightly during the annealing process.